Rapid Communication

JCBFM

Journal of Cerebral Blood Flow & Metabolism
2017, Vol. 37(3) 776–786

DOI: 10.1177/0271678X16682510
journals.sagepub.com/home/jcbfm
SAGE

^{18}F-positron-emitting/fluorescent labeled erythrocytes allow imaging of internal hemorrhage in a murine intracranial hemorrhage model

Ye Wang[1,*], Fei-Fei An[1,*], Mark Chan[1], Beth Friedman[2], Erik A Rodriguez[2], Roger Y Tsien[2,3], Omer Aras[4] and Richard Ting[1]

Abstract

An agent for visualizing cells by positron emission tomography is described and used to label red blood cells. The labeled red blood cells are injected systemically so that intracranial hemorrhage can be visualized by positron emission tomography (PET). Red blood cells are labeled with 0.3 μg of a positron-emitting, fluorescent multimodal imaging probe, and used to non-invasively image cryolesion induced intracranial hemorrhage in a murine model (BALB/c, 2.36×10^8 cells, 100 μCi, <4 mm hemorrhage). Intracranial hemorrhage is confirmed by histology, fluorescence, bright-field, and PET ex vivo imaging. The low required activity, minimal mass, and high resolution of this technique make this strategy an attractive alternative for imaging intracranial hemorrhage. PET is one solution to a spectrum of issues that complicate single photon emission computed tomography (SPECT). For this reason, this application serves as a PET alternative to [^{99m}Tc]-agents, and SPECT technology that is used in 2 million annual medical procedures. PET contrast is also superior to gadolinium and iodide contrast angiography for its lack of clinical contraindications.

Keywords

Positron emission tomography, cell tracking, optical imaging, intracranial hemorrhage, cerebral blood flow, imaging

Received 13 May 2016; Accepted 31 October 2016

Introduction

Hemorrhage is an important symptom of many diseases. Its rapid identification and repair can greatly improve patient prognosis. Unfortunately, it can be difficult to accurately image hemorrhage, especially in situations of internal bleeding. The accurate diagnosis of hemorrhage is especially vital in emergencies. This is clear in the case of stroke[1,2] where 40,000 patients per year will experience intracranial hemorrhage, and a third will die within 30 days from its complications[3,4] in the US alone. Direct, real-time monitoring of hemorrhage can improve patient outcomes, and could entail a shift in its emergency management[5] from one that is dependent on an exclusion-of-pathology process to one that capitalizes on precise and efficient diagnostic methods to inform treatment decision-making. Accurate, direct imaging of hemorrhage would help guide the surgical evaluation of a hemorrhage and prevent deterioration, brainstem compression, hydrocephalus, and supratentorial hematoma. In the case of ischemic stroke, accurate and rapid direct imaging that can exclude intracerebral

[1]Department of Radiology, Molecular Imaging Innovations Institute (MI3), New York, USA
[2]Department of Pharmacology, University of California, La Jolla, USA
[3]Howard Hughes Medical Institute, La Jolla, USA
[4]Department of Radiology, Memorial Sloan Kettering Cancer Center, New York, USA

*These authors contributed equally to this work

Co-Corresponding authors:
Richard Ting, Department of Radiology, Molecular Imaging Innovations Institute (MI3), Weill Cornell Medical College, 413 East 69th Street, New York, NY 10065, USA.
Email: rct2001@med.cornell.edu
Omer Aras, Department of Radiology, Memorial Sloan Kettering Cancer Center, New York, NY, 10065, USA.
Email: araso@mskcc.org

hemorrhage (ICH) could play a clinically important role, and potentially expand the utilization of tissue plasminogen activator (tPA) to reverse symptoms of ischemia.[6–8]

ICH in the brain is best imaged with contrast.[9] Both cerebral computed tomography angiography (CTA)[10] and magnetic resonance angiography (MRA)[11] have been used to image ICH, as they enable clear visualization of the vessels and blood pool associated with hemorrhage. Unfortunately, both CTA and MRA have clear weaknesses for emergency management. Morbidity and risk accompany angiography.[12] Patients must first be evaluated for contraindications, which take time, and inevitably, not all patients are candidates for angiography. For these reasons, CTA/MRA imaging is a foregone option in emergencies,[13] and the current standard for determining ICH and indicating intravenous tPA administration during emergencies is non-contrast CT. Unfortunately, the low sensitivity and spatial resolution of non-contrast CT can make the diagnosis of hemorrhage problematic.

Currently, most hospitals already have positron emission tomography (PET) scanners, making PET a highly promising but undervalued tool, particularly in general hemorrhage situations including acute stroke,[14] traumatic brain injury, and hematoma. There are no known life-threatening contraindications for ^{18}F-PET. PET is also directly compatible with CT, and scanners that can simultaneously acquire PET and CT are now clinically commonplace, due to the popularity of the [^{18}F]-fluorodeoxyglucose ([^{18}F]-FDG) contrast agent.[15] For imaging general hemorrhage by PET, the best contrast agent is, unironically, blood. Unlike [^{15}O]-water, and other small PET molecules, a labeled blood cell can never incorrectly indicate hemorrhage, and trigger unnecessary endoscopy/intervention, by occupying a blood-free space.[16,17] Changes in blood flow occur before metabolic and oxidative changes in tissue, making red blood cells (RBC) superior to other agents, such as [^{18}F]-FDG[18] and [^{18}F]-hypoxia sensors,[19] for imaging ICH. In addition, PET also offers a solution to a spectrum of problems that complicate single photon emission computed tomography (SPECT). [^{99m}Tc]-RBCs[20] and [^{99m}Tc]-leukocytes (exametazime)[21,22] have been applied to the imaging of stroke and intestinal/renal bleeding by SPECT. But [^{18}F]-PET is superior to SPECT because it can be used at lower doses, acquired at superior resolutions,[23,24] and is compatible with new PET/CT and PET/MR equipment. Finally, [^{18}F]-PET tracers are backward compatible with SPECT equipment,[25,26] while SPECT tracers cannot be imaged by PET.

For these reasons, we focus on developing fast, simplified chemistry for synthesizing [^{18}F]-RBCs to successfully image internal bleeding, specifically intracranial hemorrhage, by PET/CT in vivo and ex vivo.

Materials and methods

Macromolecular syntheses and characterization are described in accompanying supporting material.

RBCs isolation

Whole blood was collected from an anesthetized BALB/c mouse (3–4 week old, Charles River) by cardiac puncture in the presence of heparin as an anti-coagulant. Blood (~0.6 mL per mouse) was diluted with sterile PBS at 1:1 ratio and then layered gently onto 1.2 mL of Ficoll Paque (GE Healthcare, 17-1440-03). The mixture was then subjected to density gradient centrifugation at 190 g for 20 min at 20°C. The top and middle layers were removed by pipette carefully, leaving only the bottom, dark red, layer of RBCs. At least 10 volumes of PBS were added and the resulting mixture was centrifuged at 190 g for 30 min at 20°C to wash the RBCs. This step was repeated 6 times and was required to remove small molecules and free protein from RBCs. Supernatant was removed carefully after every centrifuge and the volume of the final RBCs solution was approximately 1 mL.

*^{18}F labeling of NHS ester **1** and **2***

In a typical radiosynthesis, an aliquot of cyclotron-proton bombarded, pure [^{18}O]-water was received and flushed with nitrogen at 28 psi in a 5.0 mL glass v-vial (Thermo Scientific Reacti-Vial #13223). The dry vial contained 67 mCi of dry activity (t = 0 min, otherwise referred to as the start of synthesis, SOS. To recover maximal activity in the referenced glass v-vial, it is important that activity is concentrated to a reduced volume but not fully evaporated). To the concentrate, ~ 5 μL volume of water, 0.8 μL of 100 mM HF (80 nmol) fluoride pH 3.0, and 4 μL of a 1 mM (20 nmol) DMSO solution of NHS esters **1** (or **2**) was added, which was heated for 1 h at 50°C. The reaction was quenched with the addition of 10 μL of a pH 6.5, 200 mM PBS solution. A 500 to 1000 μL volume of isolated RBC was added to this volume (65 min vs. SOS).

RBC labeling and workup

RBCs were labeled at room temperature with [^{18}F]-**1** for 20 min. To remove free [^{18}F]-fluoride ion and unreacted/hydrolyzed **1** or **2**, RBCs were transferred, with PBS, to a 2 mL micro centrifuge tube and centrifuged on a fixed rotor centrifuge (VWR clinical 50 centrifuge) at 190 g for 15 min. The supernatant was decanted and RBCs were transferred to 15 mL conical tubes (Falcon) along with 12 mL of 1 × PBS. Conical tubes were centrifuged on a VWR clinical 50 centrifuge for 20 min at 400 rpm (190 × g) or 1 min at 4000 rpm (190 × g) (Note that higher centrifugation speeds can lyse cells). Labeled

RBCs were washed 6 more times. This centrifugation procedure removes lysed RBCs (Supporting Figure S1), unattached fluorinated NHS ester, **1**, and free fluoride ion (Supporting Figure S3). Lysed cells do not appear after 14 h of incubation (Supporting Figure S1). A 1.6 mCi quantity of [^{18}F]-**RBC-1** was obtained on 3.78×10^9 cells in PBS, which is ready for injection into mice (1.6 mCi decay uncorrected, 5.36 mCi corrected vs. SOS). **RBC-1** was imaged using an EVOS FL auto cell imaging microscope (Life Technologies) with excitation/emission filters at 531(40)/593(40) nm respectively. **RBC-2** was imaged using excitation/emission filters at 628(40)/692(40) nm respectively.

Cryolesion model

All procedures conducted in mice were approved by the Weill Cornell Medical Center Institutional Animal Care and Use Committee (#2014-0030) and are consistent with the recommendations of the American Veterinary Medical Association and the National Institutes of Health Guide for the Care and Use of Laboratory Animals. This work is in compliance with ARRIVE guidelines for how to report animal experiments. Sixty BALB/c mice were used for this project.

A cylinder described by Raslan et al.[27] was machined for this project. The cylinder is modified to bear a tip diameter of 2.0 mm and is machined from aluminum instead of copper. The cylinder is secured in a holder fixed on an optical breadboard via a screw that allows a user to raise or lower the cryoprobe to precisely adjust contact time and force over the cryolesion-focal point. To quantitate the applied force, mice were anesthetized (2% isolfluorane/oxygen) and positioned on a scale using either 3M micropore surgical tape, or a Kopf model 900 stereotaxic instrument (images of the apparatus are shown in Supporting Figure S14).

BALB/c mice are ideal for RBC imaging because blood can be interchanged between BALB/c mice. Anesthetized BALB/c mice were disinfected twice with 70% isopropyl alcohol and 10% povidone-iodine (Betadine® Scrub). Surgical instruments were sterilized before surgery by steam sterilization and between animals using a glass bead sterilizer. An incision was made to expose the parietal bone through a 1.5 cm vertical, mid-line, cutaneous incision between the ears to create soft tissue flaps that were retracted for skull exposure in order to prepare the contact area for the cryoprobe. The cryoprobe was filled with liquid nitrogen and equilibrated for 5 min before it contacted the bare, exposed skull over the right parietal cortex of the mice (target coordinate from bregma: 1.5 mm posterior and 1.5 mm lateral). The tip of the liquid nitrogen filled cryoprobe is applied to the coordinate with a weight of 100 g (applied force 7.9 g/mm^2, over a 12.6 mm^2 surface area) as measured by scale displacement. An application time between 35 to 55 s was used. One drop of 0.25% bupivacaine solution was applied to the cryolesion site, and the incision was then closed using one or two stainless steel wound clips. The animal can be immediately transferred to an Inveon PET/CT for imaging. However, in our initial experiments, we noted that 8/30 mice perished before the end of a 40 min PET scan (55 s lesion) when we proceeded with a direct transfer from the operating table to the PET scanner. To limit mortality, we implemented a recovery step post-cryolesion where the animal was transferred from the operating table to a cage (with access to food and water) that is uniformly warmed to 25°C using a space heater. Even with longer survivals (5–6 h post cryo-lesion), no mice were lost when this recovery step is employed (over 30 mice bearing 35 s to 55 s cryolesions). This step must be performed to prevent mice from dying from hypothermia as a result of cryolesion and immediate, subsequent scanning in an Inveon PET/CT with a bore that is calibrated and run at 21°C.

[^{18}F]-PET/CT imaging of intracranial hemorrhage and scintillated biodistribution

In order to visualize intracranial bleeding, 200 μL of labeled RBC (3.76×10^8 cells, <200 μCi) were injected into the tail vein, at different time points pre- or post-cryolesion. Intracranial hemorrhage could be imaged if [^{18}F]-**RBC-1** were injected 2 h before cryolesion, up to 2 h following lesion (Supporting Figures S6, S11, S13), or 5.3 h following lesion (Supporting Figure S13). The RBC circulation time of the probe was extended by the 10 min duration for CT imaging and up to 40 min more for PET acquisition on a Siemens Inveon PET/CT. As an independent control, the cortical surface of cryolesioned brains was imaged post-mortem with white light to document the extent of surface hemorrhage. The harvested brains were also re-imaged with PET to allow spatial registration of visible hemorrhage to [^{18}F]-**RBC-1** signal. Note that the base of the brain had to be washed extensively with PBS prior to the PET scan to prevent blood pooling on the base of the scanner during imaging.

PET/CT were processed with Amide v1.0.4 and Inveon Research Workplace. Brains were frozen in Optimal Cutting Temperature (OCT) Compound (Sakura Tissue-Tec, #4585) or refrigerated in 10% paraformaldehyde PBS solution for fluorescent or histological analyses. Preservation in OCT compound is recommended if histological processing is performed after prolonged storage, i.e. >2 days, to minimize deterioration during storage (Supporting Figure S10).

Biodistribution

Acute biodistribution was determined in a separate cohort (n = 6 mice) that underwent cryolesion and RBC injection, but were not PET imaged. After cryolesion and contrast agent injection (<5 min following lesion), blood samples were collected from the left ventricle before tissues were collected for biodistribution. Scintillation measurements were taken with a Wallac Wizard 3.0 gamma counter. Mice were sacrificed by cervical dislocation before tissue was harvested. PBS or saline perfusion was not performed prior to tissue harvesting.

Biodistribution was determined by scintillated (gamma) counting. The majority of the injected [^{18}F]-**RBC-1** appears in the lung, liver, and spleen (Supporting Figure S7) as is expected for RBC biodistribution.[28] The brain accounts for approximately 1% ID/g of injected activity and does not vary between hemorrhage (0.9 ± 0.4% ID/g, SEM, n = 3) and non-hemorrhage (1.0 ± 0.2% ID/g, SEM, n = 3) bearing brains. Scintillated [^{18}F]-RBC may be greater in the lungs because blood collection was performed from the left ventricle causing blood to pool in the lungs in the short period before the organs could be harvested. The total RBC content in whole brains of mice are not significantly different in tissues of mice bearing cryolesions and mice that do not. [^{18}F]-PET is thus superior for imaging within a tissue, and for highlighting areas of local tracer maxima that are otherwise difficult to detect with imaging methods of inferior spatial resolution.

Sample size/replicates. Approximately 60 cryolesion bearing mice were used to evaluate the utility of [^{18}F]-**RBC-1** in visualizing intracranial hemorrhage. Fifteen of these mice were used as controls which were run alongside intracranial hemorrhage bearing mice. Comparisons between bright field imaging of intracranial hemorrhage-bearing tissue are shown beside comprehensive series of PET/CT sections of intracranial hemorrhage-bearing tissue in 12 mice in supporting information S13 (where the time between cryolesion and [^{18}F]-**RBC-1** injection vary between 47 min before lesion to 107 min after lesion). No two cryolesion-induced intracranial hemorrhages are identical, and volumes affected by hemorrhage differ in shape, size, path/rate of progression, and mortality. For biodistribution studies confirming that labeled RBCs distributed, according to literature,[28] two cohorts consisting of three mice each were used (Supporting Figure S7). Multiple confirmative registration techniques such as ex vivo PET, ex vivo fluorescence, ex vivo bright-field, and RBC specific TER-119 immunoperoxidase histology were used to confirm ICH.

Data blinding. The depth of a hemorrhage is difficult to know during and following cryolesion, especially since the process of cryolesion opaquely colors the skull. This phenomenon effectively randomizes our study, as the exact volume of hemorrhage becomes impossible to know until after brain excision and ex vivo PET/Brightfield/histological analysis.

Results

The primary objective of this study is the development of an imaging agent for the general observation of internal hemorrhage; specifically, intracranial hemorrhage. The chemistry chosen had to be general and applicable to all cell types in order for the imaging agent to have application to many different future cell types. For this reason, [^{18}F]-cell labeling strategies cannot employ organic co-solvents, which are cytotoxic. In recent work, we observed that the displacement of a dioxaborolane with [^{18}F]-fluoride is gentle, and that trifluoroborate synthesis proceeds in aqueous media without hydrolyzing an appended, activated N-hydroxysuccinide ester,[29] making this chemistry is uniquely suited to labeling cells. Additionally, the RBC made an ideal choice for imaging intracranial hemorrhage because, by definition, RBCs cannot occupy a blood-free space. For this reason, RBCs could be used to accurately image the porosity of the blood–brain barrier to cells and additionally distinguish hemorrhage from non-hemorrhagic edema, unlike small molecule, protein, and antibody surrogates for hemorrhage.

Timeline

The general timeline for RBC labeling was as follows: [^{18}F]-**1** synthesis (0–55 min), RBC labeling 20 min, RBC preparation and washing (20–100 min). [^{18}F]-**RBC-1** could be prepared from compound **1** in 60 to 150 min using the reported unoptimized procedures following receipt of concentrated [^{18}F]-water.

RBC labeling: In vitro studies

To demonstrate definitively that RBCs could be stably labeled with an [^{18}F]-bearing compound, it was necessary to first synthesize two small-molecule reagents, compounds **1** and **2**, for RBC labeling (Figure 1). Compounds **1** and **2** bear two fluorescent moieties that are structurally similar, but require different wavelengths for visualization.[30] Compounds **1** and **2** react in water with three equivalents of aqueous hydrogen [^{18}F]-fluoride at pH 3.0 to give N-hydroxysuccinimide (NHS) activated trifluoroborates of **1** and **2**. These agents are visible by PET,[31,32] are

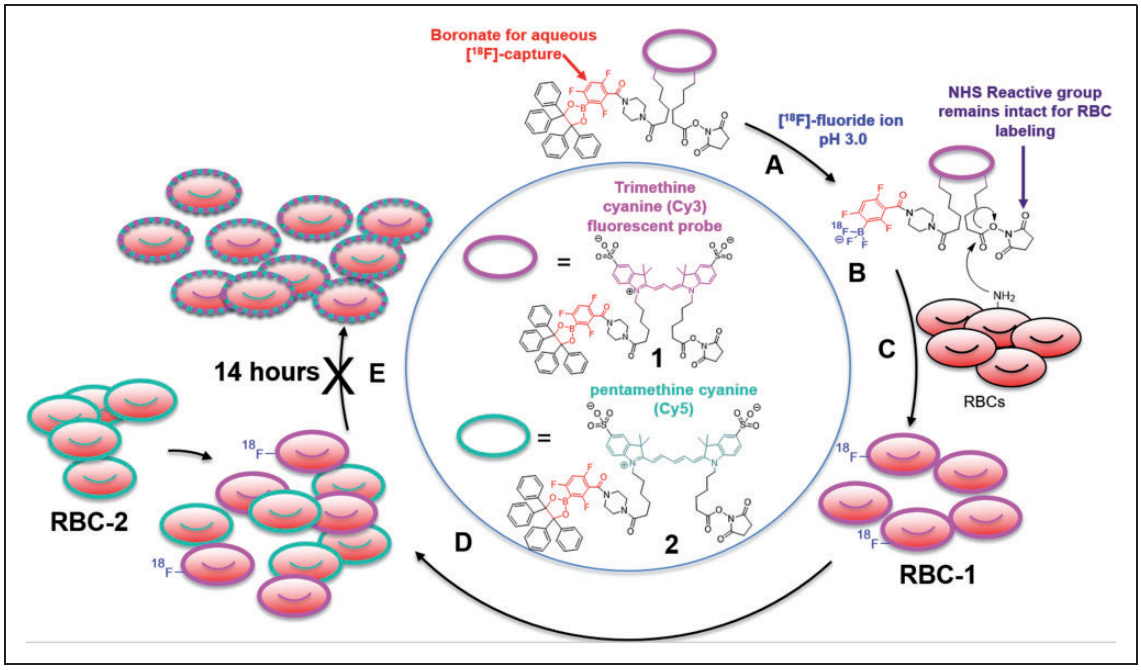

Figure 1. Structure of [^{18}F]-PET/fluorescent probes, RBC reactivity, and a scheme for demonstrating [^{18}F]-RBC stability. (a) The amine reactive ^{18}F-PET/NIRF precursor, **1**, is reacted with aqueous, [^{18}F]-fluoride at pH 3.0, to create (b) a PET imageable [^{18}F]-trifluoroborate with an intact, RBC-reactive NHS ester. (c) Free amines (typically lysine) on the surface of RBCs react with the NHS ester on **1** to give amide labeled **RBC-1**. (d) Mixing **RBC-1** with **RBC-2** create two fluorescently distinguishable populations. (e) **RBC-1** and **RBC-2** mixtures are stable for 14 h, which is confirmed by no observed dye transfer in fluorescence microscopy. Fluorophores and ^{18}F on **RBC-1** and **RBC-2** do not transfer between cells, implying that RBCs will stably retain their label in vivo.

stable in vivo,[33,34] and bear a reactive group for RBC-membrane labeling.

Once an RBC is labeled with **1** or **2**, resulting **RBC-1** or **RBC-2** do not lose or transfer their fluorophore (and, by covalent association, an [^{18}F]-label) to neighboring cells even after 14 h of incubation. This is demonstrated by mixing a batch of murine BALB/c RBCs that were labeled with **1** (**RBC-1**) with a batch of RBCs labeled with **2** (**RBC-2**), at 25°C, for 14 h. **RBCs** labeled with **1** were not visible in the Cy5 fluorescence channel used to image **2** (visibility would indicate transfer of **2** onto **RBC-1**) and vice versa (RBCs bearing **2** could not be visualized in the Cy3 fluorescence channel) at 1.5 (Supporting Figure S1) or 14-h post-incubation (Figure 2).

These data prove that fluorophores do not degrade, excrete, or exchange between cells in timeframes that are relevant to [^{18}F]-PET imaging. Additionally, these data suggest that RBC bearing **1** or **2** cannot incorrectly indicate hemorrhage through the transfer of probe to non-RBC tissue in vivo. Finally, these data also predict the stable and general extension of this technology to other cells including WBCs, platelets, circulating-tumor-cells, and T-cells for investigating initial distribution.

The labeling of RBCs with **1** and **2** does not affect RBC viability (Supporting Figure S2). Additionally, cell labeling is not observed in the presence of fetal bovine serum (FBS), demonstrating that a covalent-amide-membrane protein linkage is necessary for labeling (the high amine content of FBS, forces compound **1** to preferentially react with FBS, thus depleting the pool of NHS-activated **1** that is available to react with RBC). Compound **1** is nontoxic to glial cells (Supporting Figure S8). Compounds **1** and **2** do not transfer from RBCs into other tissues, including neighboring RBCs. The distribution of **1** on a RBC is homogeneous and uniform (Figure 2). For these reasons, we focus on **RBC-1** for in vivo studies.

[^{18}F]-RBC radiochemistry

[^{18}F]-RBCs suitable for PET imaging were synthesized in a one-vessel, two-step aqueous reaction without the use of cytotoxic organic co-solvent. In prototypical radiolabeling, compound **1** (20 nmol, 28 μg) was mixed with a 60 mCi dose of [^{18}F]-fluoride ion and a stoichiometric (3:1) quantity of fluoride at pH 3.0 in a vented vial and concentrated to a minimal volume under nitrogen flow, and heated for 1 h at 50°C. This

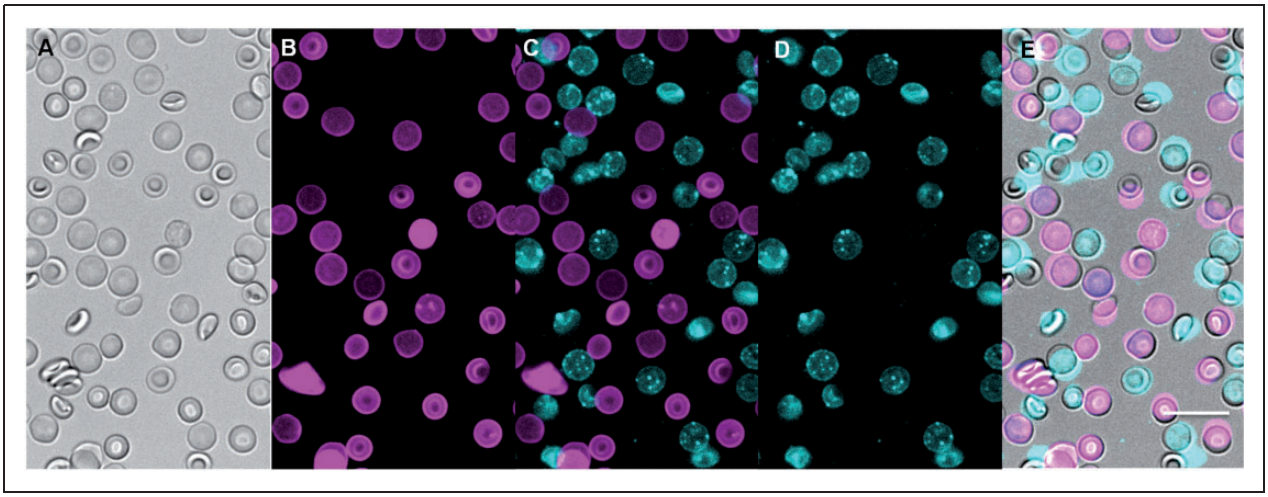

Figure 2. [^{18}F]-PET/fluorescent probes **1** (Cy3, magenta) and **2** (Cy5, cyan) can generally and stably label cells. RBCs labeled with compound **1** or **2** are mixed and incubated at 25°C for 14 h. The fluorophore is not transferred when mixed. (a) Bright field imaging of a **RBC-1/RBC-2** mixture. (b) **RBC-1** imaged with excitation/emission of 531(40)/593(40) nm, respectively. (c) Overlay of (b) and (d) showing lack of spectral overlap between the two fluorophores, and no mixing of fluorophores between cells after 14 h. (d) **RBC-2** imaged with excitation/emission of 628(40)/692(40) nm, respectively. (e) An overlay of bright field (a) and fluorescent images (c). Clearly, RBCs are not fixed due to worries that fixation agents would affect probe uptake/transfer. Scale bar = 10 μm.

radiolabeling (30 to 55 min) does not trigger major NHS hydrolysis. This reaction was neutralized to physiological pH using phosphate-buffered saline (PBS) before RBCs were immediately added to give [^{18}F]-**RBC-1**. After 20 min at room temperature, [^{18}F]-**RBC-1** was washed manually with PBS by centrifugation in order to remove [^{18}F]-fluoride ion and unreacted/hydrolyzed **1**. A 1.6 mCi quantity of [^{18}F]-**RBC-1** (3.78×10^9 cells) was isolated, ready for injection. This dose was sufficient for 16 mice (100 μCi, 2.36×10^8 RBC per mouse, 120 min).

The lower specific activity (SA) limit per molecule of **1** on [^{18}F]-**RBC-1** was 80 mCi/μmol (decay uncorrected). Each RBC contains up to 3.2 million copies of **1** (2.5×10^{11} Ci/μmol of RBC). [^{18}F]-**RBC-1** cell viability was confirmed by microscopic inspection for discocyte morphology.[35] Control experiments show that RBCs do not take up [^{18}F]-fluoride non-specifically, and that PET labeling requires boron-specific ^{18}F-capture (Supporting Figure S3).

Internal hemorrhage model

Klatzo et al.[36] reports a closed-skull, cryolesion-based model for generating traumatic brain injury (TBI) in feline models. Raslan et al.[27] has recently transformed this model in mice. By contacting the skull with a machined, liquid-nitrogen-filled aluminum probe, non-lethal, intracranial hemorrhage could be directed to chosen regions of the brain. The model does not penetrate the skull, and is superficial, allowing us to immediately corroborate [^{18}F]-**RBC-1**-PET imaging with optical photography and fluorescent imaging (Supporting Figure S4).

We identify the ideal time and contact weight that should be used with the 2.0 mm cryoprobe in 3- to 4-week-old BALB/c mice. A contact weight of 100 g should be applied to the skull at 1.5 mm posterior and 1.5 mm lateral vs. bregma[27] for a time between 35 and 55 s. In studies where insufficient contact is applied (less than 35 s) mice frequently do not develop hemorrhage, develop low-volume lesions that scab, or develop hemorrhage does not penetrate further than 1 mm in depth (determined ex vivo by macroscopic dissection). Non-hemorrhage and low volume hemorrhage cannot be imaged by [^{18}F]-**RBC-1**. In cases where excessive contact time is applied (exceeding 55 s), mice do not survive long following cryolesion. Death resulting from long contact times is observed in the absence of [^{18}F]-**RBC-1** (Supporting Figure S9, no-probe controls). It is noted that these specimens do not die on the operating table, but shortly after the procedure, suggesting that death may associated with the progression of the hemorrhage. Shorter (35 s) cryoprobe contact times expectedly result in smaller hemorrhagic volumes as confirmed in ex vivo analyses (compare Supporting Figure S13f,g (35 s) to Supporting Figures S11 and S13h-l (55 s)).

A contact time that approaches 55 s has never failed to generate intracranial hemorrhage, and for this reason, is the preferred contact time for [^{18}F]-**RBC-1** studies. Mice can survive for a significant amount of

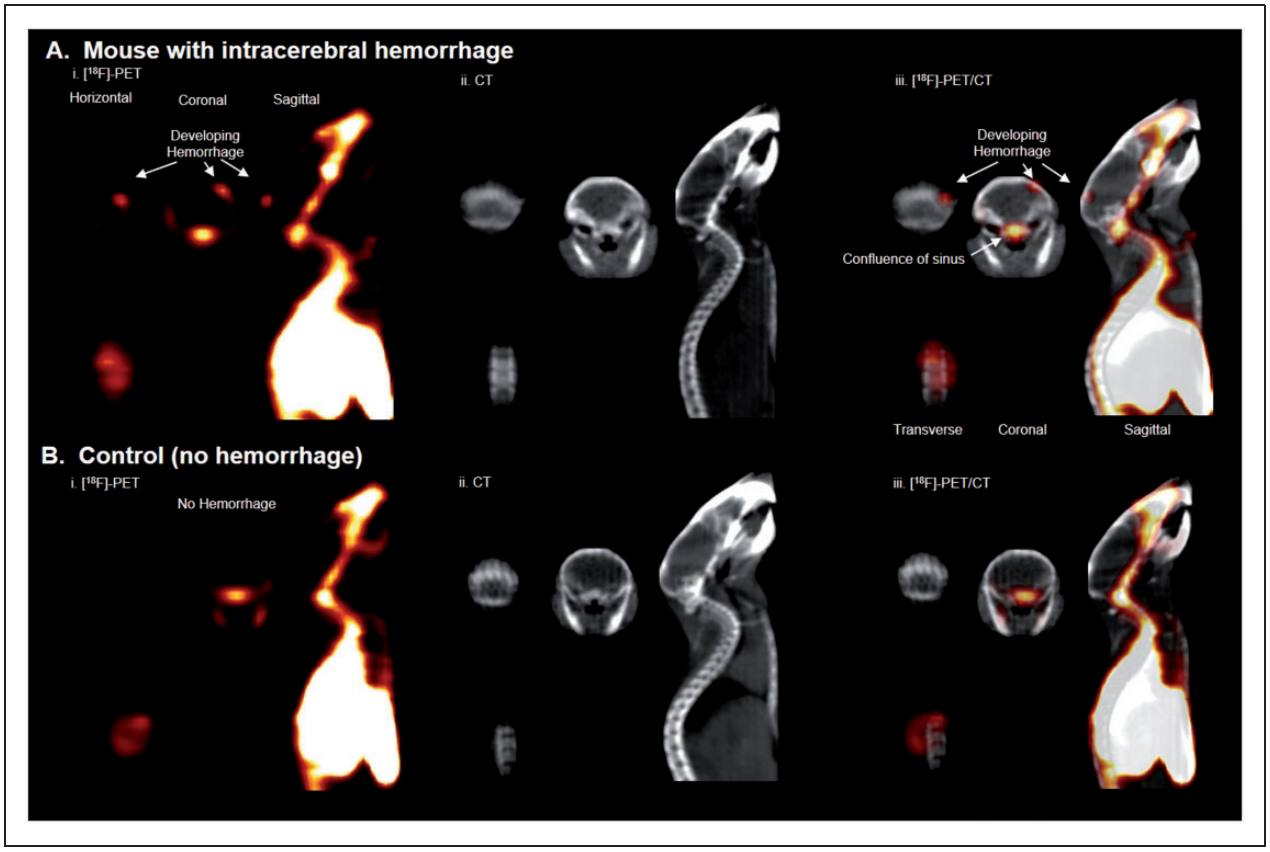

Figure 3. Intracranial hemorrhage is visualized with [^{18}F]-**RBC-1** non-invasively, in a full body [^{18}F]-PET scan. (a) Mouse with brain hemorrhage 10–40 min after [^{18}F]-**RBC-1** i.v. injection. (i) PET (compiled image from 10 to 40 min), (ii) CT, and (iii) PET/CT scans. Hemorrhage is indicated by white arrow and is visualized by PET, but not CT. (b) Mouse without brain hemorrhage after [^{18}F]-**RBC-1** i.v. injection. (i) PET (compiled image from 10 to 40 min), (ii) CT, and (iii) PET/CT scans. PET signal is not visible in the brain of control mouse, (b).

time following cryolesion if a recovery step is immediately employed. Following cryolesion, mice must be disconnected from isoflurane anesthesia, and immediately transferred to a cage, with food and water, that is heated to 25°C using a space heater. The recovery to normal body temperature in these awakened mice eliminates mortality from continued anesthetization (isofluorane) and subsequent mouse scanning on the Inveon PET/CT, which has an imaging bore that is normally, calibrated, conditioned and run at 21°C.

[^{18}F]-RBC animal imaging

Six mice were imaged with [^{18}F]-**RBC-1** injection prior to cryolesion. Twenty-five mice were imaged with [^{18}F]-**RBC-1** 0–120 min post cryolesion, and six mice were injected with [^{18}F]-**RBC-1** contrast ~5 h post cryolesion. Twenty mice were used without cryolesion, with [^{18}F]-**RBC-1**, as controls.

Pairs of BALB/c mice were injected with 100 μCi (3.78×10^8 RBCs) of [^{18}F]-**RBC-1** in 200 μL PBS through the tail vein. One of each mouse pairs received a cryolesion before mouse pairs were transferred to an Inveon PET/CT and imaged by CT (10 min) followed by PET (40 min, note that a full 40 min was performed but is not required).

Hemorrhage at the site of cryolesion was clearly visible by whole body PET, showing that [^{18}F]-**RBC-1** could be used to non-invasively image intracranial hemorrhage in mice. PET activity corresponding to hemorrhage was asymmetric, localized to the site of cryolesion (Figure 3, Supporting Video S1), and was not present in control mice that do not bear hemorrhage (Supporting Video S2).

To confirm that the activity of interest is indeed due to hemorrhage, mice were sacrificed following scanning, and the brains of both cryolesion and control mice were excised, photographed (white light), and imaged again, ex vivo by PET/CT. Bright field imaging showed hemorrhage near the surface of the brain at the site of cryolesion (Figure 4(a)). The dimensions and asymmetric, anatomical location of ICH were corroborated by PET imaging (Figure 4(b), Supporting Video S3). Fluorescence confirmed intracranial hemorrhage in

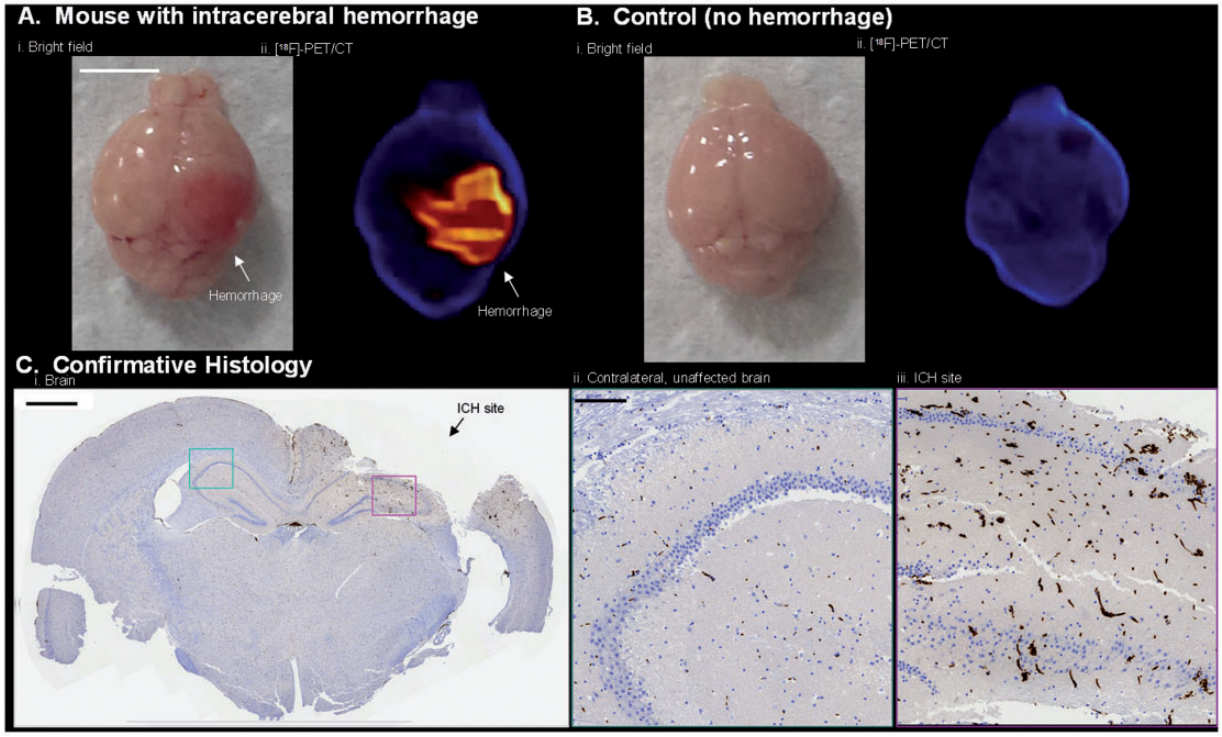

Figure 4. [^{18}F]-RBC-1, located at the hemorrhage site, is imaged by [^{18}F]-PET ex vivo and verified by histology. (a) Ex vivo: (i) Bright field and (ii) PET/CT images of intracranial hemorrhage in brain specimen from Figure 3(a). Images acquired 60 min after cryolesion. (b) Ex vivo: (i) Bright field and (ii) PET/CT images of brain without intracranial hemorrhage from Figure 3(b). Scale bar = 0.5 cm. (c) Formalin-fixed paraffin, 5 μm coronal section of brain in (a) stained with RBC-specific TER-119 antibody, hematoxylin, and eosin. (i) Whole brain section with intracranial hemorrhage site shown with black arrow. Scale bar = 0.1 cm. (ii) Contralateral tissue without hemorrhage and (iii) hemorrhage site magnified 10× of cyan and magenta sections, respectively, in c(i). In (iii), vessels are enlarged, irregular, and increased in frequency. Scale bar is or = 0.01 cm. (c, i-iii) RBC staining is shown in brown by oxidation of diaminobenzidine by secondary Ab labelled with horseradish peroxidase.

the brain ex vivo (Supporting Figure S4). Tissue disintegration and major RBC washout were observed in attempts at preserving brain for confirmative MRI (Supporting Figure S5); however, hemorrhage was confirmed in formalin-fixed paraffin sections of brain with RBC-specific, TER-119 immunohistochemical staining (Figure 4(c)). Tissue disintegration can be avoided by storing tissue in OCT compound at −78°C (Supporting Figure S10).

[^{18}F]-**RBC-1** can be injected both before (Figures 3 and 4) and after lesion (10 to 100 min, Supporting Figures S6, S11, and S13) to image intracranial hemorrhage. Longer temporal delays could be inserted between cryolesion and [^{18}F]-**RBC-1** injection without affecting the ability to image intracranial hemorrhage (Supporting Figures S6 and S11). However, when longer delays are inserted (5.3 h), visible, ex vivo hematoma, do not match PET data as precisely (Supporting Video S4, compare Supporting Figure S12 (5.3 h) with Supporting Figures S6 and S11 (2 h or less)). This may be due to changes in blood flow at the cryolesion site that result in differing local rates of active hemorrhage. General biodistribution data correspond to what is expected of RBCs in a rodent[28] (Supporting Figure S7). The observation of minimal RBC in the intestine (lower-GI) is perhaps, the most significant result, implying that [^{18}F]-**RBC-1** can be used as a general probe for imaging hemorrhage and future development can be used to generate [^{18}F]-PET alternatives to SPECT-agents.

Discussion

Experimental design

The primary objective of this study was the development of a universal imaging agent for observing active hemorrhage. The chemistry chosen must be general and applicable to all cell types in order for the imaging agent to have application to many diseases, and to be of interest to a general scientific community. It is preferred that [^{18}F]-cell labeling strategies that do not

employ organic co-solvents, which are cytotoxic, and are preferred by biologists and clinicians. The RBC made an ideal choice for imaging hemorrhage because, by definition, RBCs cannot occupy a blood-free space. RBCs could be used to additionally distinguish hemorrhage from edema, unlike [^{18}F]-small molecules, proteins, and antibodies.

A disease model had to be chosen in order to demonstrate an imaging sensitivity that is superior to existing SPECT technology. Of all internal bleeding models, the ICH model produces the maximum degree of morbidity and mortality from minimal volumes of bleeding and is therefore more difficult to image than other models of internal bleeding. When significant delays are inserted between cryolesion and [^{18}F]-**RBC-1** contrast injection (Supporting Figure S12), visible, ex vivo hematoma begin to match [^{18}F]-**RBC-1** PET data less precisely (~millimeter resolution, Supporting Video S4). This mismatch may reflect local differences in hemorrhagic rates resulting from attempts by a specimen to recover from cryogenic hemorrhage (e.g. clotting). In translation, this [^{18}F]-**RBC-1** PET data, may delineate regions of active bleeding from inactive/less-active hemorrhage in situations that might not be obvious by CTA/MRA.

[^{18}F]-**RBC-1** facilitates PET imaging of intracranial hemorrhage at a very high resolution. Images are higher in resolution then current clinical SPECT imaging.[20–22] The sub-microgram (trace) doses required in imaging [^{18}F]-**RBC-1** ensure that this PET technique does not suffer from contraindications that plague CTA and MRA (e.g. nephrogenic systemic fibrosis). Unlike CTA and MRA, a patient can be injected with [^{18}F]-**RBC-1** and then transferred directly from an ambulance into a PET/CT without the need for intermediate screening. In non-emergency, general internal hemorrhage situations, [^{18}F]-**RBC-1** can help monitor hemorrhagic progression and response to intervention, especially in patients with challenged renal function. PET does not interfere with MRA and CTA, allowing one to additionally contemplate confirmative, combined, [^{18}F]-**RBC-1**-PET/CTA or PET/MRA imaging applications.

There are no major foreseeable barriers to having [^{18}F]-**RBC-1** serve as an immediate imaging alternative to [^{99m}Tc]-agents in the clinic. Human type O-negative blood is easy to obtain. Patients with non-emergent, suspected cases of renal and intestinal bleeding are scanned regularly with [^{99m}Tc]-agents in preparation for surgery. Most hospitals have PET/CTs. Facilities that handle ^{18}F-FDG synthesis are more than equipped to handle the described radiosynthesis. The greater goal of using [^{18}F]-**RBC-1** as a general tool for imaging general internal bleeding in the emergency department (ED) is more ambitious. Although most hospitals have PET/CTs, EDs do not have on-demand access to PET/CTs. Many EDs do have CTs, and PET and CT share many instrumentation aspects; therefore, PET/CTs do not require a hospital to assign additional space or shielding, nor would it be a paradigm shift to have CTs upgraded to PET/CTs in the ED. The ability to have [^{18}F]-**RBC-1** ready on demand is more problematic. The time-consuming process in [^{18}F]-**RBC-1** preparation is the post-synthetic separation of [^{18}F]-**RBC-1** from [^{18}F]-fluoride ion. These issues could be accounted for through pre-emptive delivery of O-negative RBC (200 mL) pre-labeled as [^{18}F]-**RBC-1** at high activity. [^{18}F]-**RBC-1** synthesis via microwave reaction or RBC containment and purification by continuous flow centrifugation (in an apheresis unit) could also produce [^{18}F]-**RBC-1** on demand. Additionally, modified centrifugation methods would reduce the period of [^{18}F]-**RBC-1** separation from [^{18}F]-fluoride ion and lysed RBC, from minutes to seconds.[37,38]

In this application, the fluorescent component on [^{18}F]-**RBC-1** and [^{18}F]-**RBC-2** play a passive, but vital role in demonstrating stable, non-transferrable RBC-labeling in vitro, and confirmation of hemorrhage in the brain ex vivo. In clinical ICH imaging, the presence of the skull and overlying tissue would reduce fluorophore utility. The fluorescent component of the [^{18}F]-RBC would be superior to stand-alone, [^{18}F]-PET-only imaging agents in endoscopic procedures.[39] In more advanced applications, especially non-cerebral ones, [^{18}F]-**RBC** fluorescence would be useful in intestinal bleeding, renal bleeding, and other internal bleeding, where fluorophores would guide a surgeon to a fluorescent probe in real-time, high-resolution, fluorescence-guided surgical repair.[40,41] In the case that a surgical site is saturated with blood, a second, different-colored-fluorophore-containing-RBC (**RBC-2**) can be used to freshly image a bleed in a different fluorescent channel.

In conclusion, we report a small-molecule multimodality PET/fluorescent cell labeling reagent that is used to label RBCs. The fluorescent component of this probe is used to show that labeled RBCs do not transfer their probe to other tissues (read other RBCs) even after 14 h of incubation. The PET component of the probe is used to successfully image active intracranial hemorrhage, in vivo, in live mice. This is confirmed by ex vivo PET, fluorescence, and histology.

Funding

The author(s) disclosed receipt of the following financial support for the research, authorship, and/or publication of this article: The project is supported by grants to R.Y.T. from the US National Institutes of Health (CA158448) and the Howard Hughes Medical Institute. R.T. is funded by the National Institute of Biomedical Imaging and

Bioengineering K99/R00 (EB013904). O.A. is funded in part through the NIH/NCI Cancer Center Support Grant P30 CA008748.

Acknowledgments

This study is dedicated to the memory of Roger Y Tsien.

Declaration of conflicting interests

The author(s) declare no potential conflicts of interest with respect to the research, authorship and or publication of this article.

Authors' contributions

RYT, OA, BF, and RT designed the study. BF, YW, FA, and RT generated animal models. FA and MC performed chemical syntheses. YW and EAR performed in vitro cell labeling studies. YW, FA, and RT performed RBC isolation. Radiolabeling was done by YW, FA, and RT. OA acquired histology. RYT, OA, RT, EAR, and BF contributed to the editing and writing of the manuscript. All authors contributed to the discussion of the methods and animal models.

Supplementary material

Supplementary material for this paper can be found at http://journals.sagepub.com/doi/suppl/10.1177/0271678X16682510

References

1. Pendlebury ST. Worldwide under-funding of stroke research. *Int J Stroke* 2007; 2: 80–84.
2. Leak RK, Zheng P, Ji X, et al. From apoplexy to stroke: historical perspectives and new research frontiers. *Prog Neurobiol* 2014; 115: 1–5.
3. Sacco S, Marini C, Toni D, et al. Incidence and 10-year survival of intracerebral hemorrhage in a population-based registry. *Stroke* 2009; 40: 394–399.
4. Gebel JM and Broderick JP. Intracerebral hemorrhage. *Neurol Clin* 2000; 18: 419–438.
5. Morgenstern LB, Hemphill JC III, Anderson C, et al. Guidelines for the management of spontaneous intracerebral hemorrhage: a guideline for healthcare professionals from the American Heart Association/American Stroke Association. *Stroke* 2010; 41: 2108–2129.
6. Wardlaw JM, Murray V, Berge E, et al. Recombinant tissue plasminogen activator for acute ischaemic stroke: an updated systematic review and meta-analysis. *Lancet (London, England)* 2012; 379: 2364–2372.
7. Brown MD, Burton JH, Nazarian DJ, et al. Clinical policy: Use of intravenous tissue plasminogen activator for the management of acute ischemic stroke in the emergency department. *Ann Emerg Med* 2015; 66: 322–333.e31.
8. Darkhabani Z, Nguyen T, Lazzaro MA, et al. Complications of endovascular therapy for acute ischemic stroke and proposed management approach. *Neurology* 2012; 79: S192–S198.
9. Huisman TGM. Intracranial hemorrhage: ultrasound, CT and MRI findings. *Eur Radiol* 2005; 15: 434–440.
10. Zhu XL, Chan MSY and Poon WS. Spontaneous intracranial hemorrhage: Which patients need diagnostic cerebral angiography? A prospective study of 206 cases and review of the literature. *Stroke* 1997; 28: 1406–1409.
11. Dumoulin CL and Hart HR Jr. Magnetic resonance angiography. *Radiology* 1986; 161: 717–720.
12. Heiserman JE, Dean BL, Hodak JA, et al. Neurologic complications of cerebral angiography. *AJNR Am J Neuroradiol* 1994; 15: 1401–1407, discussion 8–11.
13. Jagoda AS, Bazarian JJ, Bruns JJ Jr., et al. Clinical policy: neuroimaging and decisionmaking in adult mild traumatic brain injury in the acute setting. *Ann Emerg Med* 2008; 52: 714–748.
14. Bunevicius A, Yuan H and Lin W. The potential roles of 18F-FDG-PET in management of acute stroke patients. *Biomed Res Int* 2013; 2013: 634598.
15. Buck AK, Herrmann K, Stargardt T, et al. Economic evaluation of PET and PET/CT in oncology: Evidence and methodologic approaches. *J Nucl Med Technol* 2010; 38: 6–17.
16. Volpe JJ, Herscovitch P, Perlman JM, et al. Positron emission tomography in the newborn: Extensive impairment of regional cerebral blood flow with intraventricular hemorrhage and hemorrhagic intracerebral involvement. *Pediatrics* 1983; 72: 589–601.
17. Vlasenko A, Petit-Taboue MC, Bouvard G, et al. Comparative quantitation of cerebral blood volume: SPECT versus PET. *J Nucl Med* 1997; 38: 919–924.
18. Dethy S, Goldman S, Blecic S, et al. Carbon-11-methionine and fluorine-18-FDG PET study in brain hematoma. *J Nucl Med* 1994; 35: 1162–1166.
19. Sarrafzadeh AS, Nagel A, Czabanka M, et al. Imaging of hypoxic-ischemic penumbra with (18)F-fluoromisonidazole PET/CT and measurement of related cerebral metabolism in aneurysmal subarachnoid hemorrhage. *J Cereb Blood Flow Metab* 2010; 30: 36–45.
20. Sakai F, Igarashi H, Suzuki S, et al. Cerebral blood flow and cerebral hematocrit in patients with cerebral ischemia measured by single-photon emission computed tomography. *Acta Neurol Scand* 1989; 80: 9–13.
21. Soucy JP, McNamara D, Mohr G, et al. Evaluation of vasospasm secondary to subarachnoid hemorrhage with technetium-99m-hexamethyl-propyleneamine oxime (HM-PAO) tomoscintigraphy. *J Nucl Med* 1990; 31: 972–977.
22. Moretti JL, Defer G, Cinotti L, et al. Luxury perfusion'' with 99mTc-HMPAO and 123I-IMP SPECT imaging during the subacute phase of stroke. *Eur J Nucl Med* 1990; 16: 17–22.
23. Rischpler C, Park MJ, Fung GS, et al. Advances in PET myocardial perfusion imaging: F-18 labeled tracers. *Ann Nucl Med* 2012; 26: 1–6.
24. Tsien RY. Imagining imaging's future. *Nat Rev Mol Cell Biol* 2003; Suppl: SS16–SS21.
25. Zeng GL, Gullberg GT, Bai C, et al. Iterative reconstruction of fluorine-18 SPECT using geometric point response correction. *J Nucl Med* 1998; 39: 124–130.
26. Knesaurek K and Machac J. Comparison of 18F SPECT with PET in myocardial imaging: a realistic thorax-

cardiac phantom study. *BioMed Central Nucl Med* 2006; 6: 5–12.
27. Raslan F, Albert-Weißenberger C, Ernestus R-I, et al. Focal brain trauma in the cryogenic lesion model in mice. *Exp Transl Stroke Med* 2012; 4: 1–6.
28. Šebestík V, Brabec V, Jelínek J, et al. Red cell, plasma and whole blood volumes in organs of normal and hypersplenic rats. *Blut* 1974; 29: 203–209.
29. Rodriguez EA, Wang Y, Crisp JL, et al. New dioxaborolane chemistry enables [(18)F]-positron-emitting, fluorescent [(18)F]-multimodality biomolecule generation from the solid phase. *Bioconj Chem* 2016; 27: 1390–1399.
30. Mujumdar RB, Ernst LA, Mujumdar SR, et al. Cyanine dye labeling reagents: sulfoindocyanine succinimidyl esters. *Bioconjug Chem* 1993; 4: 105–111.
31. Liu ZB, Pourghiasian M, Radtke MA, et al. An organotrifluoroborate for broadly applicable one-step F-18-labeling. *Angew Chem-Int Ed* 2014; 53: 11876–11880.
32. Ting R, Adam MJ, Ruth TJ, et al. Arylfluoroborates and alkylfluorosilicates as potential PET imaging agents: high-yielding aqueous biomolecular 18F-labeling. *J Am Chem Soc* 2005; 127: 13094–13095.
33. Ting R, Aguilera TA, Crisp JL, et al. Fast 18F labeling of a near-infrared fluorophore enables positron emission tomography and optical imaging of sentinel lymph nodes. *Bioconjug Chem* 2010; 21: 1811–1819.
34. Ting R, Harwig C, auf dem Keller U, et al. Toward [F-18]-labeled aryltrifluoroborate radiotracers: In vivo positron emission tomography imaging of stable aryltrifluoroborate clearance in mice. *J Am Chem Soc* 2008; 130: 12045–12055.
35. Diez-Silva M, Dao M, Han J, et al. Shape and biomechanical characteristics of human red blood cells in health and disease. *MRS Bull* 2010; 35: 382–388.
36. Klatzo I, Piraux A and Laskowski EJ. The relationship between edema, blood-brain-barrier and tissue elements in a local brain injury. *J Neuropathol Exp Neurol* 1958; 17: 548–564.
37. Lew VL and Ferreira HG. Variable Ca sensitivity of a K-selective channel in intact red-cell membranes. *Nature* 1976; 263: 336–338.
38. Garcia-Sancho J and Lew VL. Detection and separation of human red cells with different calcium contents following uniform calcium permeabilization. *J Physiol* 1988; 407: 505–522.
39. Herance JR, Gispert JD, Abad S, et al. Erythrocytes labeled with [18F]SFB as an alternative to radioactive CO for quantification of blood volume with PET. *Contrast Media Mol Imaging* 2013; 8: 375–381.
40. Wu AP, Whitney MA, Crisp JL, et al. Improved facial nerve identification with novel fluorescently labeled probe. *Laryngoscope* 2011; 121: 805–810.
41. An F-F, Chan M, Kommidi H, et al. Dual PET and near-infrared fluorescence imaging probes as tools for imaging in oncology. *Am J Roentgenol* 2016; 207: 266–273.